Technology and Health Care 24 (2016) S849–S858 S849
DOI 10.3233/THC-161215
IOS Press

Study of human walking patterns based on the parameter optimization of a passive dynamic walking robot

Xizhe Zang, Xinyu Liu*, Yanhe Zhu and Jie Zhao
State Key Laboratory of Robotics and System, Harbin Institute of Technology, Harbin, Heilongjiang, China

Abstract.
BACKGROUND: The study of human walking patterns mainly focuses on how control affects walking because control schemes are considered to be dominant in human walking.
OBJECTIVE: This study proposes that not only fine control schemes but also optimized body segment parameters are responsible for humans' low-energy walking.
METHODS: A passive dynamic walker provides the possibility of analyzing the effect of parameters on walking efficiency because of its ability to walk without any control. Thus, a passive dynamic walking model with a relatively human-like structure was built, and a parameter optimization process based on the gait sensitivity norm was implemented to determine the optimal mechanical parameters by numerical simulation.
RESULTS: The results were close to human body parameters, thus indicating that humans can walk under a passive pattern based on their body segment parameters. A quasi-passive walking prototype was built on the basis of the optimization results. Experiments showed that a passive robot with optimized parameters could walk on level ground with only a simple hip actuation.
CONCLUSION: This result implies that humans can walk under a passive pattern based on their body segment parameters with only simple control strategy implying that humans can opt to walk instinctively under a passive pattern.

Keywords: Human walking, passive dynamic walking, parameters optimization, energy consumption

1. Introduction

Humans walk efficiently and capably on even ground with a natural gait (inverted pendulum-like gait), exhibiting low-energy consumption, high stability, and significant versatility. In recently years, researchers have attempted to better understand human walking to create more sophisticated walking rehabilitation equipment. Three approaches are typically used to study human walking gait characteristics and energy consumption (i.e., walking patterns).

The first approach is to observe and measure human walking, and then calculate and analyze how walking speed and joint torque affect walking patterns [1–3]; this is a direct method.

*Corresponding author: Xinyu Liu, State Key Laboratory of Robotics and System, Harbin Institute of Technology, Harbin, Heilongjiang, China. Tel.: +86 0451 86414538; Fax: +86 0451 86413392; E-mail: wo-shiliuxinyu@163.com.

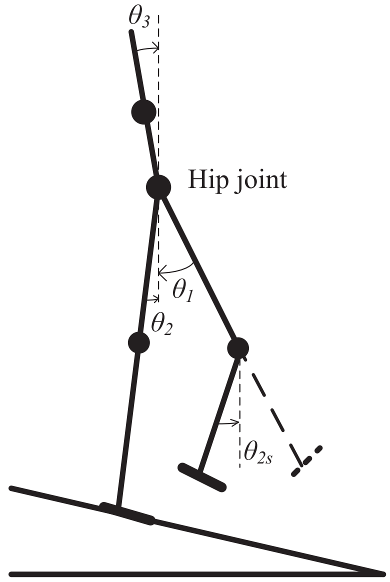

Fig. 1. PDW model.

The second approach is to build a human neuromusculoskeletal model [4] to calculate and simulate human walking. Then, it is possible to calculate and optimize how muscle forces and limb motions affect walking efficiency.

The third approach is to build a robot that can mimic human walking. However, traditional active walking robots such as Asimo [5] walk with high-energy consumption [6] and an unnatural gait because of the static control method based on the ZMP method [7], which is unsuitable for analyzing human walking. Passive dynamic walking (PDW) proposed by McGeer [8] provides a new way to build robots with human-like gaits and low-energy consumption; these models can be used as a new approach to studying human walking patterns.

All three approaches evaluate how control affects walking patterns without considering the effects of body segment parameters on walking efficiency. Inspired by passive dynamic walking, this study evaluates whether human body parameters play a role in walking to save walking energy, and studies human walking patterns based on the optimization parameters of a passive dynamic walking robot.

2. Modeling and dynamics

2.1. Walking model

In this study, we built a relatively human-like PDW model composed of an upper body, a hip, two knees, and two ankle joints. This model could descend a gentle slope without any control, as shown in Fig. 1. The walking motion was restricted in the sagittal plane (i.e., two links were fixed together to form one leg to avoid lateral falling) because the lateral dynamics (e.g., scrubbing torques, rolling, and collisions) were difficult to simulate. A kinematic coupling mechanism kept the upper body centered between the two legs by [9].

As shown in Fig. 2, the human walking cycle can be divided into four phases.

Table 1
Physical parameters of the PDW model

Parameters	Descriptions	Dimensionless processes	Dimensionless parameters
l_t	Thigh length	l_t/l	k_{lt}
b_t	Center of mass of the thigh	$b_t/l_t \cdot (l_t/l)$	$K_{bt} \cdot k_{lt}$
b_s	Center of mass the shank	$b_s/l_s \cdot (l_s/l)$	$K_{bs} \cdot (1\text{-}k_{lt})$
b_b	Center of mass of the body	b_b/l	K_{bb}
m_h	Hip mass	m_h/M	K_{mh}
m_t	Thigh mass	m_t/M	k_{mt}
m_s	Shank mass	m_s/M	k_{ms}
m_b	Upper body mass	m_b/M	k_{mb}
l_f	Foot length	l_f/l	K_{lf}
r_f	Ratio between back-foot and fore-foot	/	/
t	time	$t/(l/g)^{1/2}$	τ

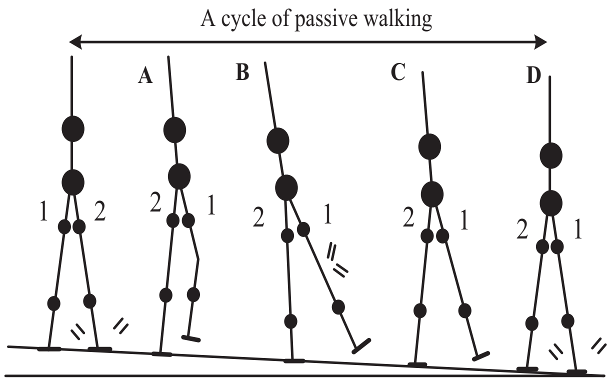

Fig. 2. One typical walking cycle of a PDW model.

Phase (A): Four-rods walking phase. The leading thigh can freely rotate forward around the hip joint, and the shank can also freely rotate around the knee joint.
Phase (B): Four-rods locking phase. When the leading thigh swings to a certain position (before foot-ground impact), the knee joints can be locked by a locking mechanism to prevent bending after the foot impacts the floor.
Phase (C): Three-rods walking phase. The thigh and shank straighten without a bend at the knee. This leg continues to rotate forward.
Phase (D): Three-rods impacting phase. The leading straight leg impacts the floor when the feet touch the floor to become the new trailing leg. The walking step ends at this point.

2.2. *Walking dynamics*

Table 1 shows the physical parameters and their dimensionless forms. The parameters can be divided by M (total masses of the PDW model) or l (straight-leg length) to create a dimensionless form for easier calculation and comparability.

This model can be described by the generalized coordinate q_i. Three degree of freedoms (DOFs) were observed in Phase (A). Therefore, the generalized coordinates were $q_i = [\theta_1, \theta_2, \theta_{2s}]^T$. The bisecting mechanism always constrained the upper body in the middle of the two legs as $\theta_3 = (\theta_1 + \theta_2)/2$.

The walking dynamics could be described by the Lagrange equation. The Phase (A) walking dynamics can be written as follows:

$$Mf_1(\dot\theta_1,\dot\theta_2,\dot\theta_{2s},\theta_1,\theta_2,\theta_{2s})\ddot\theta = Ff_1(\dot\theta_1,\dot\theta_2,\dot\theta_{2s},\theta_1,\theta_2,\theta_{2s}) + S\tau \tag{1}$$

In Eq. (1), $Mf_1(\theta)$ are the inertia matrixes; $Ff_1(\theta)$ are the Coriolis forces and gravity matrixes; τ is the torques imposed in each DOF. Equation (1) is an ordinary differential equation set. The walking dynamics can be solved with a Matlab ODE45 integrating process.

During Phase (B), we assume that both the knee locking and the foot-ground impact are handled as instantaneous and fully-inelastic impacts in which no bounces or slips occur, and the joint angles cannot change at that moment. The thigh and shank are combined to form a new leg because of the knee locking, decreasing the system variables from 6 to 4. During knee locking, the angular momentum of the leading leg is conserved around the hip joint, and the angular momentum of the entire robot is conserved around the tailing leg foot-ground contact point O, as follows:

$$\begin{aligned}&\overrightarrow{L_O^+}(\theta_1^+,\theta_2^+,\dot\theta_1^+,\dot\theta_2^+) = \overrightarrow{L_O^-}(\theta_1^-,\theta_2^-,\theta_{2s}^-,\dot\theta_1^-,\dot\theta_2^-,\dot\theta_{2s}^-)\\&\overrightarrow{L_H^+}(\theta_1^+,\theta_2^+,\dot\theta_1^+,\dot\theta_2^+) = \overrightarrow{L_H^-}(\theta_1^-,\theta_2^-,\theta_{2s}^-,\dot\theta_1^-,\dot\theta_2^-,\dot\theta_{2s}^-)\end{aligned} \tag{2}$$

The knee locking should meet Eq. (3) as well:

$$\theta_1^+ = \theta_1^-, \theta_2^+ = \theta_2^- = \theta_{2s}^- \tag{3}$$

Equation (2) is rearranged into the following generalized form:

$$\begin{bmatrix} af_{11} & af_{12} \\ af_{21} & af_{22}\end{bmatrix}\begin{bmatrix}\dot\theta_1^+ \\ \dot\theta_2^+\end{bmatrix} = \begin{bmatrix} bf_{11} & bf_{12} & bf_{13} \\ bf_{21} & bf_{22} & bf_{23}\end{bmatrix}\begin{bmatrix}\dot\theta_1^- \\ \dot\theta_2^- \\ \dot\theta_{2s}^-\end{bmatrix} \tag{4}$$

We can use Eqs (3) and (4) to determine the state variable values after the foot-ground impact, which could be applied as the starting state values of the next phase.

The dynamics of Phase (C) follow the same form as Phase (A), except that the DOFs of the model decrease to 2. Therefore, the generalized coordinates are $q_i = [\theta_1, \theta_2]^T$. The walking equation of Phase (C) is:

$$\begin{bmatrix} m_{11}f_{11} & m_{12}f_{12} \\ m_{21}f_{21} & m_{22}f_{22}\end{bmatrix}\begin{bmatrix}\ddot\theta_1 \\ \ddot\theta_2\end{bmatrix} = \begin{bmatrix} ff_1(\theta_1,\theta_2,\dot\theta_1,\dot\theta_2) \\ ff_2(\theta_1,\theta_2,\dot\theta_1,\dot\theta_2)\end{bmatrix} \tag{5}$$

During the foot-ground impact in Phase (D), the angular momentum of the new leading leg is conserved around the hip joint and the angular momentum of the entire robot around the impact point I is as follows:

$$\begin{aligned}&\overrightarrow{L_I^+}(\theta_1^+,\theta_2^+,\dot\theta_1^+,\dot\theta_2^+) = \overrightarrow{L_I^-}(\theta_1^-,\theta_2^-,\dot\theta_1^-,\dot\theta_2^-)\\&\overrightarrow{L_H^+}(\theta_1^+,\theta_2^+,\dot\theta_1^+,\dot\theta_2^+) = \overrightarrow{L_H^-}(\theta_1^-,\theta_2^-,\dot\theta_1^-,\dot\theta_2^-)\end{aligned} \tag{6}$$

The foot-ground impact must also meet the conditions of Eq. (7) because the leading leg becomes the trailing leg and vice versa.

$$\theta_1^+ = \theta_2^-, \theta_{2s}^+ = \theta_2^+ = \theta_1^-, \dot\theta_{2s}^+ = \dot\theta_2^+ \tag{7}$$

Equations (6) and (7) are rearranged into the following generalized form:

$$\begin{bmatrix} af_{11} & af_{12} \\ af_{21} & af_{22}\end{bmatrix}\begin{bmatrix}\dot\theta_1^+ \\ \dot\theta_2^+\end{bmatrix} = \begin{bmatrix} bf_{11} & bf_{12} \\ bf_{21} & bf_{22}\end{bmatrix}\begin{bmatrix}\dot\theta_1^- \\ \dot\theta_2^-\end{bmatrix} \tag{8}$$

Due to space limitations, this paper does not list the details of the coefficient matrixes.

Table 2
Optimization results

k_{bb}	k_{bt}	k_{bs}	k_{lt}	r_f
0.3–0.32	0.31–0.32	0.48–0.5	0.49–0.5	0.42–0.44
l_f	k_{mt}	k_{mh}	k_{ms}	k_{mb}
0.28	0.09–0.11	0.27–0.29	0.05–0.06	0.39–0.41

3. Parameters optimization and results

3.1. Numerical simulation process

A numerical simulation was performed using Matlab to determine a stable walking gait and optimized parameters. After being provided with the proper starting state values, the PDW robot can stably walk down a gentle slope. The time immediately after foot-ground impact became the start and end points of the walking cycle because the number of independent state parameters decreased to 3, which decreases computing time. Phase (A) was integrated numerically by the ODE45 method in Matlab until the running program detected the knee locking event of Phase (B), and then the locking process was computed on the basis of angular momentum conservation. Next, Phase (C) was integrated by the ODE45 method until the program detected the foot-ground impact event of Phase (D), and then the impact process was computed. A walking cycle simulation ended when the foot impacted the ground. The state variables immediately after impact were used as the initial conditions of the next step. If the initial conditions converged to one point, the passive walking robot would walk with the same gait in every step. This condition is called limit cycle walking, and the point is called the fixed point.

3.2. Parameters optimization and results

The gait sensitivity norm method [10] was selected as mechanical parameter optimization criterion because it showed a suitable correlation with actual disturbance rejection, and had a short calculation time. The gait sensitivity norm calculation details are presented in [10]. The lower the gait sensitivity norm value, the better the robot coul reject disturbances. Therefore, the reciprocal of the gait sensitivity norm $1/\|\partial g/\partial e\|_2$ was selected as mechanical parameter optimization criterion in the direct analysis.

The passive model could walk on a certain slope using the initial condition $q_0 = [-0.2000, 0.3200, 0.1400]^T$. The parameter optimization process was performed as follows: the numerical simulation process began by using the initial condition q_0 under a combination of certain parameters obtained from previous knowledge. A parameter to be optimized was carefully changed in each step; the other parameters remained constant. The gait sensitivity norm was then calculated. After 10-step simulations (if all steps were successful), the parameter value that led to the highest reciprocal of the gait sensitivity norm value was selected as the optimized parameter. The other parameters were optimized through the same process. The simulation was manually restarted whenever the robot fell.

As shown in Fig. 3, walking stability first increased and then decreased as k_{bs}, k_{lt}, k_{bt}, and k_{bb} increased. k_{bb} obtained the best walking stability at approximately 0.3. k_{bt} obtained the best walking stability at approximately 0.32. Both k_{bs} and k_{lt} obtained the best walking stability at approximately 0.5. The COM position of the upper body k_{bb} was the most sensitive to walking stability.

Figure 4 shows the effects of r_f and l_f on the gait sensitivity norm. The walking stability first grew and then decreased as r_f increased. r_f obtained the best walking stability at approximately 0.42. r_f was the least sensitive to walking stability when $l_f = 0.28$.

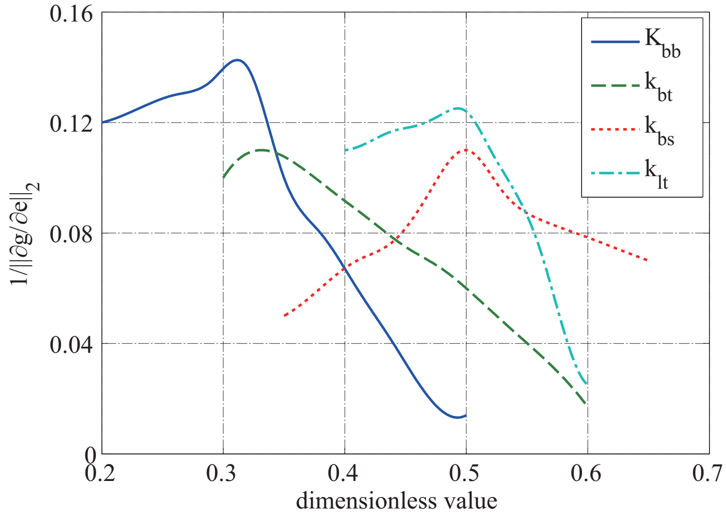

Fig. 3. Effects of k_{bs}, k_{lt}, k_{bt}, and k_{bb} on the gait sensitivity norm.

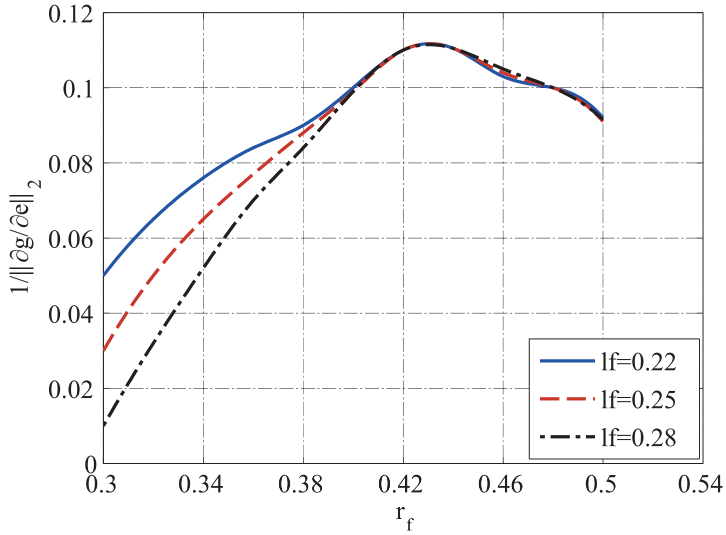

Fig. 4. Effects of r_f and l_f on the gait sensitivity norm.

In Fig. 5, walking stability first grew and then decreased as k_{mt} k_{ms}, k_{mh}, and k_{mb} increased. k_{mt} obtained the best walking stability at approximately 0.1. k_{ms} obtained the best walking stability at approximately 0.05. k_{mh} obtained the best walking stability at approximately 0.28. k_{mb} obtained the best walking stability at approximately 0.4.

Figure 6 shows the limit cycle of the swing leg using the optimized parameters, indicating that the swing leg can rapidly converge to its limit cycle, and that walking was stable.

Table 2 shows the parameter optimization results. The results were near the parameters measured in [11], indicating that humans can walk under passive patterns that use their body parameters.

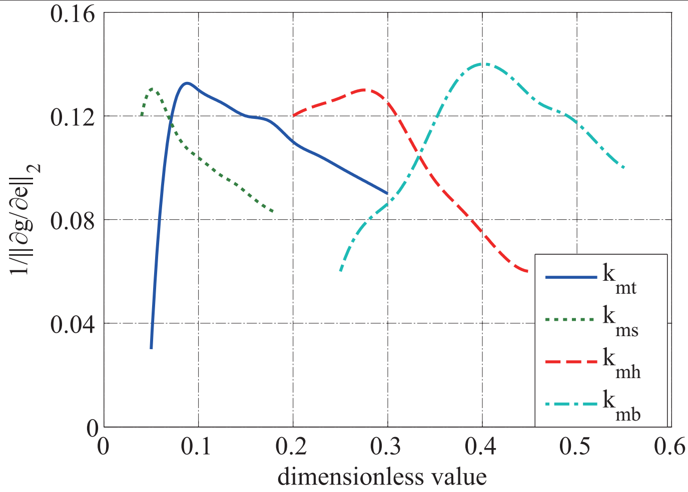

Fig. 5. Effects of k_{mt} , k_{ms}, k_{mh}, and k_{mb} on gait sensitivity norm.

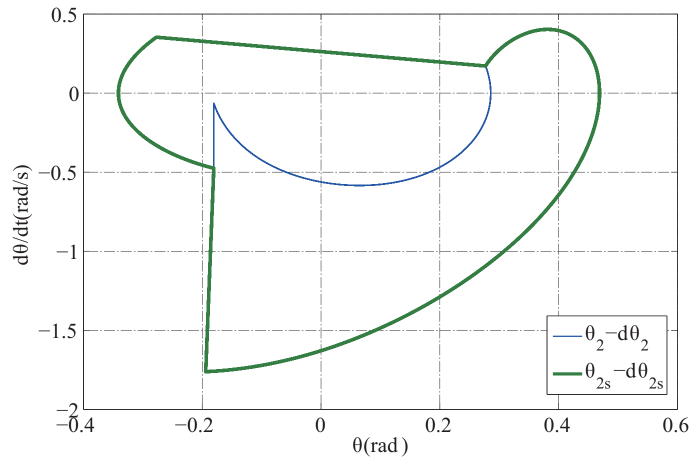

Fig. 6. Limit cycle of the swing leg.

4. Experiments

4.1. System overview of prototype

A mechanical prototype (Fig. 7) was built to determine if the passive robot could use its parameters on level ground.

The prototype had five DOFs. A locking mechanism was installed on each knee joint to lock or release the leading leg by a solenoid. A DC servo motor installed at the upper body was connected to two antagonistically connected linear springs through cables to make a series of elastic actuators (SEA) [12] (Fig. 7), which was a flexible driving element that worked in a fashion similar to human muscles. This flexible element was essential for passive robots using their own parameters to walk, as the traditional driving pattern significantly impeded walking by immediately stopping motion whenever the driving

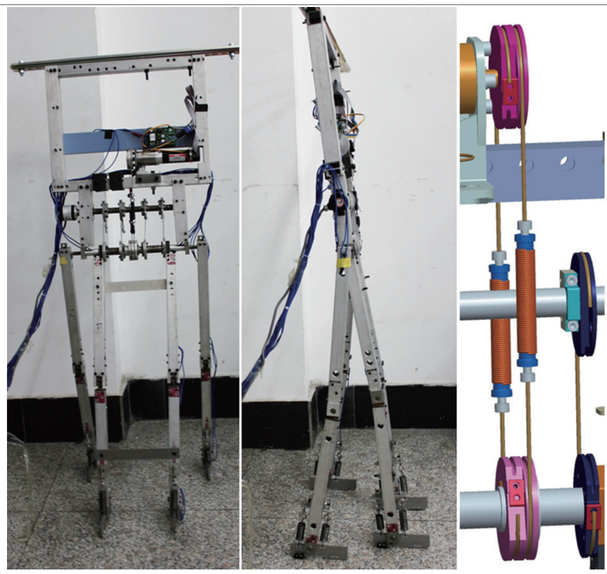

Fig. 7. Prototype and SEA model in Pro/E.

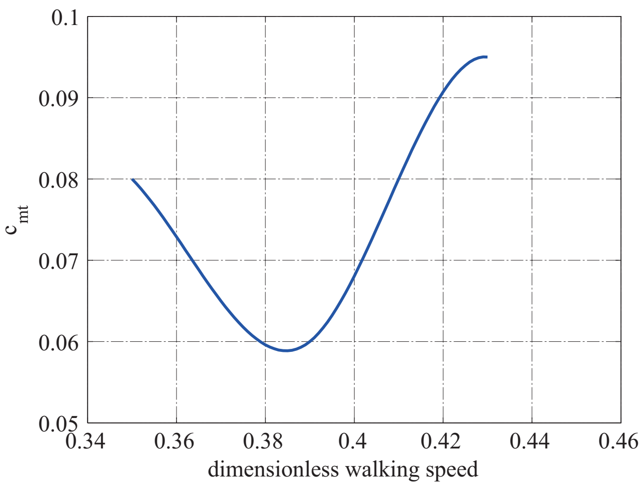

Fig. 8. Speed change effect on mechanical cost of transport.

stopped. This driving element could also be achieved by pneumatic muscles or other flexible structures [13]. A PCI data acquisition card and a digital amplifier of the DC motor were connected to a PC; they exchanged data with the PC to finish the auto-control walking.

4.2. Experiments

The passive walker stably walked on a level floor using a simple PD control scheme in Eq. (9) at the hip joint, as shown in Fig. 9.

$$\tau_s = -K_p(\theta - \theta^d) - K_d\dot{\theta} \tag{9}$$

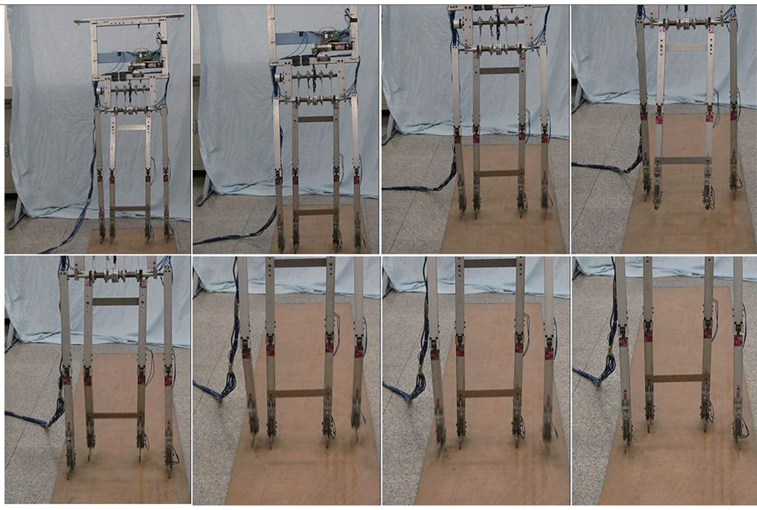

Fig. 9. Walking experiment frames.

The mechanical cost of transport, as defined in Eq. (10), was calculated in each step to analyze the energy consumption of the prototype during walking (i.e., S is the step length).

$$c_{mt} = \left(\sum_{i=1}^{n} \int_{0}^{T} |\tau.\dot{\phi}_i|.dt \right) /mg.S \tag{10}$$

The mechanical cost of transport was calculated using data collected from sensors at the DC motor and hip joint, as shown in Fig. 8. The robot obtained the lowest mechanical cost of transport of 0.06 at the speed of 0.39, which was slightly higher than that of humans. This condition was probably caused by a lack of complex control during impact. The robot walked stably with low-energy consumption using only simple control at the hip joint. Therefore, saving energy through passive dynamics is relatively simple. Seeking efficiency is part of human nature, so humans are likely to walk under passive patterns to save energy.

5. Conclusion and discussion

The results of the passive robot parameter optimization and prototype experiments showed that humans are likely to walk under passive patterns because body parameters play an important role in saving energy. The reasons for this condition are discussed as follows:

(1) Human body parameters are similar to those of an optimized passive robot; thus humans should similarly use their body parameters. Human optimized body parameters may be the result of natural selection.

(2) Humans can master their body parameters more easily than can robots. Paired with the fact that humans tend to favor efficient methods by nature, humans can use their optimized body parameters to increase walking efficiency.

Evidence of human passive walking patterns can also be found in [14]; humans were found to consume the lowest energy when walking at a speed of 80 m/min. That tendency is relatively consistent with our experimental results. Only one walking pattern can be generated passively for certain body parameters. Energy has to be consumed to change such pattern (i.e., changing the walking speed).

Humans do not only walk under passive patterns. Human can generate more complex walking patterns under unique circumstances, such as when falling. However, humans prefer passive walking patterns during free walking on level ground to save energy. Evidence suggests that when a ground height change is unrecognized, humans immediately lose balance as passive walking patterns are still performed.

Future work will focus on examining more walking patterns by adding more controls to the prototype.

Acknowledgments

This study is funded by National Magnetic Confinement Fusion Science Program “Multi-Purpose Remote Handling System with Large-Scale Heavy Load Arm” (2012GB102004).

References

[1] Kautz S A, Bowden M G, Clark D J, et al., Comparison of motor control deficits during treadmill and overground walking poststroke[J], Neurorehabilitation and neural repair, 2011, 25(8): 756-765.
[2] Paul J P, History and fundamentals of gait analysis, Bio-medical materials and engineering, 1999, Vol. 8(3-4), pp. 123-35.
[3] Q. Sun, R. Ma, F. Hu and Q. Hao, Space Encoding Based Human Activity Modeling and Situation Perception, In Proceeding of 2013 IEEE International Multi-Disciplinary Conference on Cognitive Methods in Situation Awareness and Decision Support, 2013, pp. 186-189.
[4] Anderson F C, Pandy M G, Dynamic optimization of human walking[J], Journal of biomechanical engineering, 2001, 123(5): 381-390.
[5] Y. Sakagami, R. Watanabe, C. Aoyama, S. Matsunaga, N. Higaki, K. Fujimura, The Intelligent Asimo: System Overview and Integration, 2002 IEEE/RSJ International Conference on Intelligent Robots and Systems, Lausanne, Switzerland, 2002: 2478-2483.
[6] Collins S H, Ruina A, A bipedal walking robot with efficient and human-like gait[C]//Robotics and Automation, 2005, ICRA 2005, Proceedings of the 2005 IEEE International Conference on, IEEE, 2005: 1983-1988.
[7] M. Vukobratovic, B. Borovac, Zero-Moment Point-Thirty Five Years of Its Life, Int J Hum Robot, 2004, 1(1): 157-173.
[8] T. McGeer, Passive Dynamic Walking, International Journal of Robotics Research, 1990, 9(2): 62-82.
[9] Wisse M, Hobbelen D G E, Schwab A L, Adding an upper body to passive dynamic walking robots by means of a bisecting hip mechanism[J], Robotics, IEEE Transactions on, 2007, 23(1): 112-123.
[10] Hobbelen D G E, Wisse M, A disturbance rejection measure for limit cycle walkers: The gait sensitivity norm[J], Robotics, IEEE Transactions on, 2007, 23(6): 1213-1224.
[11] Wells J P, DeMenthon D F, Measurement of body segment mass, center of gravity, and determination of moments of inertia by double pendulum in Lemur fulvus[J], American Journal of Primatology, 1987, 12(3): 299-308.
[12] Pratt G A, Williamson M M, Series elastic actuators[C]//Intelligent Robots and Systems 95. Human Robot Interaction and Cooperative Robots, Proceedings. 1995 IEEE/RSJ International Conference on. IEEE, 1995, 1: 399-406.
[13] Li J, Ji Z, Shi X, et al., Design and optimization of multi-class series-parallel linear electromagnetic array artificial muscle[J], Bio-medical materials and engineering, 2014, 24(1): 549-555.
[14] Ralston H J, Energetics of Human Walking, in: Neural Control of Locomotion, R.M. Herman et al., eds, Plenum Press, New York, 1976, pp. 77-98.